doi:10.1016/j.jmb.2011.06.009 J. Mol. Biol. (2011) 411, 321–328

Contents lists available at www.sciencedirect.com

Journal of Molecular Biology

journal homepage: http://ees.elsevier.com.jmb

COMMUNICATION

Molecular Basis of a Million-Fold Affinity Maturation Process in a Protein–Protein Interaction

Daniel A. Bonsor[1], Sandra Postel[1], Brian G. Pierce[2], Ningyan Wang[3], Penny Zhu[1], Rebecca A. Buonpane[3], Zhiping Weng[2], David M. Kranz[3] and Eric J. Sundberg[1]*

[1]*Boston Biomedical Research Institute, 64 Grove Street, Watertown, MA 02472, USA*
[2]*Program in Bioinformatics and Integrative Biology, University of Massachusetts Medical School, Worcester, MA 01605, USA*
[3]*Department of Biochemistry, University of Illinois Urbana-Champaign, Urbana, IL 61801, USA*

Received 7 April 2011;
received in revised form
2 June 2011;
accepted 4 June 2011
Available online
12 June 2011

Edited by I. Wilson

Keywords:
protein–protein interactions;
protein engineering;
yeast display;
X-ray crystallography;
computational biology

Protein engineering is becoming increasingly important for pharmaceutical applications where controlling the specificity and affinity of engineered proteins is required to create targeted protein therapeutics. Affinity increases of several thousand-fold are now routine for a variety of protein engineering approaches, and the structural and energetic bases of affinity maturation have been investigated in a number of such cases. Previously, a 3-million-fold affinity maturation process was achieved in a protein–protein interaction composed of a variant T-cell receptor fragment and a bacterial superantigen. Here, we present the molecular basis of this affinity increase. Using X-ray crystallography, shotgun reversion/replacement scanning mutagenesis, and computational analysis, we describe, in molecular detail, a process by which extrainterfacial regions of a protein complex can be rationally manipulated to significantly improve protein engineering outcomes.

Modern molecular biology techniques have greatly accelerated the use of recombinant biological molecules in the clinic.[1] Accordingly, therapeutic proteins now comprise one of the most important and fastest-growing sectors of pharmaceutical development. Recombinant proteins have provided novel therapeutic options for a wide range of human diseases, including those for which no drugs produced by more traditional chemistry-based methods exist.

Many proteins, however, are unsuitable as therapeutic molecules in their naturally occurring state. Protein engineering methods provide routes to achieve a wide array of desired properties. One of the most popular and effective engineering techniques is to subject a protein of interest to an evolutionary process.[2–4] The power of protein evolution derives from its ability to select variants with a desired property (in particular, improved binding affinity) from a highly diverse pool. Using such methods for directed evolution, we can

*Corresponding author. Institute of Human Virology and Department of Medicine, University of Maryland School of Medicine, Baltimore, MD 21201, USA. E-mail address: esundberg@ihv.umaryland.edu.

Present addresses: D. A. Bonsor and S. Postel, Institute of Human Virology, University of Maryland School of Medicine, Baltimore, MD 21201, USA; R. A. Buonpane, MedImmune, Gaithersburg, MD 20878, USA.

Abbreviations used: CDR, complementarity-determining region; TCR, T-cell receptor; SAG, superantigen; mVβ8.2, mouse TCR Vβ8.2; SEB, staphylococcal enterotoxin B; hVβ2.1, human TCR Vβ2.1; SpeC, streptococcal pyrogenic exotoxin C.

engineer recombinant proteins to bind a nearly limitless repertoire of potential targets with relatively high specificity and affinity.

Mammalian immune systems are encoded with natural protein engineering tools. Antibodies, as products of the adaptive immune system, are exceptionally well suited for combating infectious diseases: hypervariability and a natural affinity maturation process allow for the recognition of diverse antigens;[5] a constant region triggers potent immune mechanisms. Antibodies have therefore been commonly used as therapeutic molecules, either in their natural state or after further engineering.

Alternatives to antibodies—largely in the form of diverse scaffolds for the design and engineering of recombinant proteins that often serve as high-affinity steric inhibitors of deleterious protein interactions—have been developed (reviewed by Binz *et al.*[6] and Binz and Pluckthun[7]). Like antibodies, these scaffold proteins are often able to bind a wide range of target proteins. The natural protein binding partners of drug targets, although more restricted in their specificity than generic scaffold proteins, provide additional alternatives for protein engineering that can lead to highly effective therapeutic proteins.[8–10]

Protein engineering methods have been restricted traditionally to amino acid sequence variations of the initial protein architecture, and not expansion or modification of the architecture itself. Recent studies, however, have shown that engineering strategies that dispense of natural protein architectures, through the recombination and rearrangement of protein domains and modules, can result in engineered proteins that exhibit unique molecular recognition properties and novel functions (reviewed by Koide[11]). Hybrid methods that exist somewhere between maintaining and dispensing of the initial protein architecture, by diversifying not only the sequence but also the length of protein loops within or near the protein–protein interface, have now been utilized successfully in numerous molecular systems. This is yet another engineering strategy that mimics nature, especially the length diversity of complementarity-determining region (CDR) 3 loops in antibodies and T-cell receptors (TCRs).[12] Several groups, using as scaffold the 10th type III domain of human fibronectin, which has an immunoglobin-like β-sandwich fold and CDR-like loops, have exploited loop length diversity to achieve significant affinity gains.[13–16] Here we present the detailed molecular basis of an amino acid residue and a loop length diversity protein engineering process that, when combined, resulted in a greater-than-million-fold affinity increase in an engineered TCR/superantigen (SAG) complex.

We previously used a semirational protein engineering strategy that incorporated structure-based knowledge concerning protein complexes that are homologous to the targeted complex in order to increase the extent and degree of affinity maturation.[17] We generated an engineered TCR variant named G5-8, derived from the mouse TCR Vβ8.2 (mVβ8.2) chain, that binds to the bacterial SAG staphylococcal enterotoxin B (SEB) with a 3-million-fold increase in affinity relative to the wild-type mVβ8.2, with measured binding affinities of 48 pM[17] and 150 μM,[18] respectively. Additionally, we showed that G5-8 acts as an inhibitor of SEB-mediated T-cell activation and is completely protective *in vivo* when administered to animals challenged with a lethal dose of SEB.[17] A brief overview of our semirational structure-based protein engineering strategy is presented here as a guide for the structural and energetic bases of the engineered affinity maturation described below.

Initially, following a standard directed evolution strategy, we created libraries with genetic variability in the mVβ8.2 region but without sequence length changes within the targeted mVβ8.2/SEB complex molecular interface and selected affinity-matured variants, using yeast display (Fig. 1a). Genetic diversity was focused entirely on the CDR2 loop of mVβ8.2, since it forms the majority of the protein–protein interface with SEB and contains several hot-spot contacts.[19] From this process, we generated G2-5, a variant of mVβ8.2 that binds SEB with an affinity of 650 pM,[17] an approximate 200,000-fold increase relative to the wild-type complex.

Subsequently extending from the G2-5 platform, we followed a semirational directed evolution engineering strategy (Fig. 1b) that takes advantage of the structure-based knowledge of a homologous TCR/SAG complex—the human TCR Vβ2.1 (hVβ2.1) domain in complex with streptococcal pyrogenic exotoxin C (SpeC). SpeC interacts with hVβ2.1, forming intermolecular contacts with each TCRβ hypervariable loop[20] (Fig. 1b, left), while SEB contacts only the mVβ8.2 CDR2 and HV4 loops[21] (Fig. 1a, left and middle). The CDR1 loop of hVβ2.1 includes a noncanonical single amino acid residue insertion, which acts to push several residues C-terminal to it closer to the SpeC molecular surface to make numerous intermolecular interactions that have been shown to augment the affinity of the hVβ2.1/SpeC complex.[22] Conversely, residues from the shorter CDR1 loop of mVβ8.2 are located at too great a distance from SEB to make specific interactions (Fig. 1b, middle).

With this more comprehensive structural understanding of TCR/SAG interactions and seeking to functionalize the CDR1 loop of mVβ8.2 as a meaningful contributor to increased SEB binding affinity, we extended the standard directed evolution approach (Fig. 1a, right) by generating additional mVβ8.2 libraries that included randomized CDR1 loops with either one or two additional amino acid residues relative to the wild-type sequence and

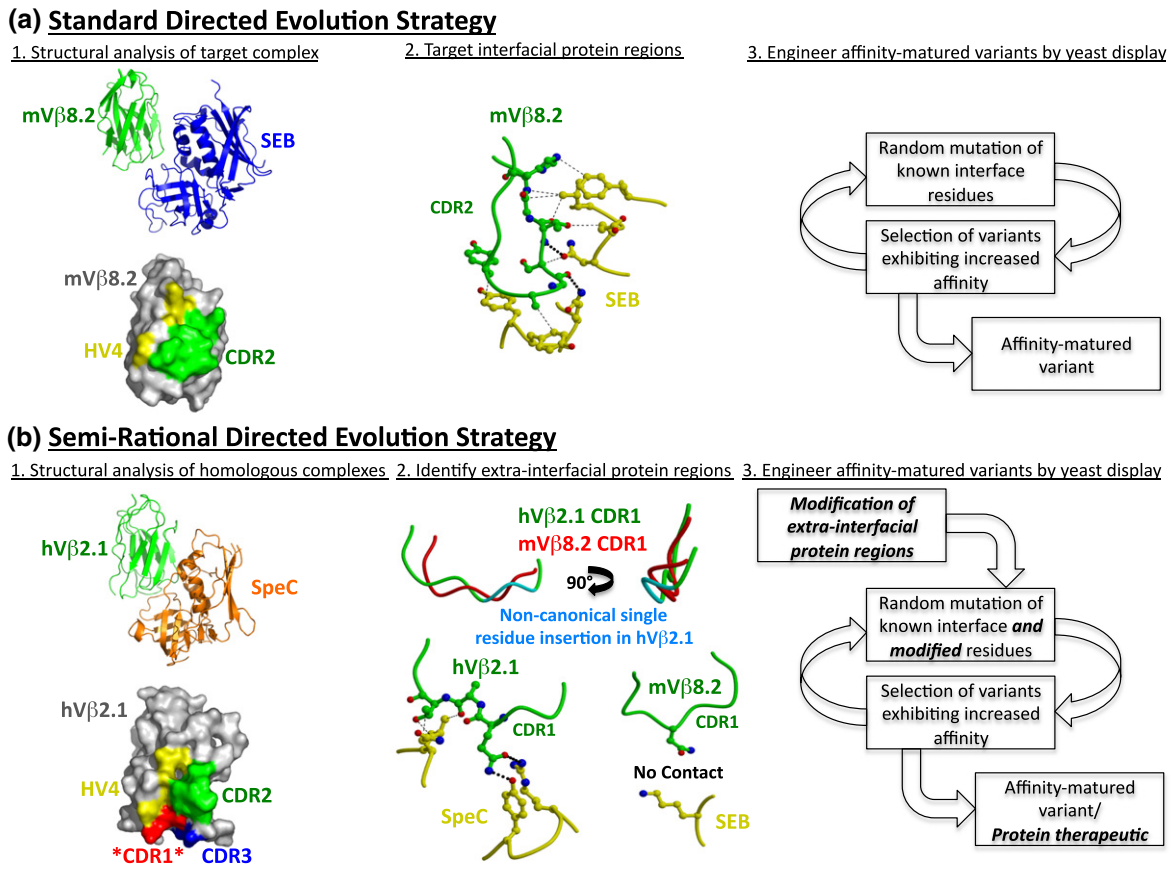

Fig. 1. Directed evolution strategies. (a) Steps in the standard directed evolution strategy. Shown are the structure of the wild-type mVβ8.2/SEB complex (top left), interacting surfaces on mVβ8.2 when bound to SEB (bottom left), close-up view of mVβ8.2 CDR2 loop interactions with SEB (middle), and the iterative process of mutagenesis and selection (right). (b) Steps in the rationalized directed evolution strategy. Shown are the structure of wild-type hVβ2.1/SpeC (top left); interacting surfaces on hVβ2.1 when bound to SpeC (bottom left); comparison of hVβ2.1 and mVβ8.2 CDR1 loop structures and intermolecular contacts with SpeC and SEB, respectively (middle); and the iterative process of mutagenesis and selection beginning with the structure-based modification of extrainterfacial residues (right).

by selecting for affinity-matured variants (Fig. 1b, right). After exhaustive iterative rounds of mutagenesis and selection for mVβ8.2 variants with a modified CDR1 loop length, most of the isolated variants contained a single additional residue. One of these, variant G5-8, incorporated the additional CDR1 loop residue (Ser27a$^{G5\text{-}8}$), as well as two CDR1 loop variant residues (Tyr28$^{G5\text{-}8}$ and Phe29$^{G5\text{-}8}$). G5-8 binds to SEB with an affinity of 48 pM,[17] 3-million-fold higher than the wild-type mVβ8.2/SEB complex and more than 10-fold higher than G2-5, the highest-affinity variant with a conserved sequence length relative to the template for directed evolution, wild-type mVβ8.2.

The structural basis of this rationalized protein engineering method is now revealed by our 2.95-Å X-ray crystal structure of the G5-8/SEB complex, combined with a mutational analysis (see Supplementary Information, Materials and Methods). Crystallographic and refinement statistics for this structure are listed in Table 1. There were eight G5-8/SEB complexes per asymmetric unit in this crystal. The interface G5-8 variant residues and the SEB residues that they contact from all of these complexes superimpose essentially perfectly (Supplementary Fig. 1), even though the noncrystallographic constraints on all interface residues were relaxed in the final stages of refinement. Electron density maps also clearly delineate the side-chain positions of these residues (Supplementary Fig. 2).

When the G5-8/SEB structure is superimposed onto the wild-type mVβ8.2/SEB structure,[21] the two main chains of the complexes are nearly indistinguishable, except for the CDR1 loops of G5-8 and mVβ8.2 (Fig. 2a). A schematic interaction map of the wild-type mVβ8.2/SEB and affinity-matured G5-8/SEB protein–protein interfaces is shown in Supplementary Fig. 3. Three G5-8 residues (Ser27a$^{G5\text{-}8}$, Tyr28$^{G5\text{-}8}$, and Phe29$^{G5\text{-}8}$) replace two

Table 1. Crystallographic and refinement statistics for the G5-8/SEB complex structure

Data collection	
Space group	$P2_12_12_1$
Unit cell parameters	
a, *b*, *c* (Å)	109.95, 160.37, 186.27
α, β, γ (°)	90.00, 90.00, 90.00
Total number of observations	917,195
Unique reflections	66,122
Resolution (Å)	121.53–2.95 (3.06–2.95)
R_{sym}	0.199 (0.793)
$I/\sigma I$	16.75 (4.5)
Completeness (%)	94.7 (99.0)
Redundancy	13.9 (13.8)
Refinement statistics	
Reflections used	61,375
Number of residues in asymmetric unit	2698
Number of ligands in asymmetric unit	39
R_{work} (%)	24.6
R_{free} (%)	26.6
RMS bond lengths (Å)	0.01
RMS bond angles (°)	1.26
Average *B*-factors	
Protein	
SEB	45.8
G5-8	40.6
Ligands	50.0
Ramachandran plot statistics	
Most favored regions (%)	88.7
Additionally allowed regions (%)	10.3
Generously allowed regions (%)	0.7
Disallowed regions (%)	0.3

mVβ8.2 residues (Asn28$^{mV\beta8.2}$ and His29$^{mV\beta8.2}$), resulting in a longer CDR1 loop with a distinct conformation (Fig. 2b). The structural effect of these CDR1 loop sequence and length changes in G5-8 is that the side chain of Tyr28$^{G5\text{-}8}$ is pointed directly toward SEB (Fig. 2c), confirming the rational basis of our engineering strategy.

Mutations in the CDR2 loop of G5-8, which are similar to those in G2-5, include two relatively large amino acid side chains that replace minimal side chains. These include substitutions of Ala52$^{mV\beta8.2}$ and Gly53$^{mV\beta8.2}$ with Ile52$^{G5\text{-}8}$ and Arg53$^{G5\text{-}8}$, respectively (Fig. 2d). Together, the variant CDR1 and CDR2 loop residues in G5-8 that make intermolecular contacts with SEB (Tyr28$^{G5\text{-}8}$, Ile52$^{G5\text{-}8}$, and Arg53$^{G5\text{-}8}$) encompass the β-sandwich domain of SEB, extending from the interdomain cleft to its periphery (Fig. 2c), a well-documented region of energetic importance for TCR/SAG complexes.[19,23]

The variant residues in G5-8 from both the CDR1 loop and the CDR2 loop form numerous intermolecular contacts with SEB that are absent in the wild-type mVβ8.2/SEB complex. This results in relative increases in buried TCR surface area (805 Å^2 *versus* 561 Å^2), shape complementarity (0.67 *versus* 0.56), and hydrogen bonds (11 *versus* 3). The CDR1 loop mutation Tyr28$^{G5\text{-}8}$ forms a pi-stacking interaction with Arg110^{SEB} and a hydrogen bond with Asn60^{SEB} (Fig. 2e). This results in an additional ~70 Å^2 of buried surface area that is not present in the mVβ8.2/SEB complex. The CDR2 loop mutations Ile52$^{G5\text{-}8}$ and Arg53$^{G5\text{-}8}$ form van der Waals contacts and a hydrogen bond with a trio of SEB asparagine residues (Asn31^{SEB}, Asn60^{SEB}, and Asn88^{SEB}). These three variant residues in the G5-8 CDR1 (Tyr28$^{G5\text{-}8}$) and CDR2 (Ile52$^{G5\text{-}8}$ and Arg53$^{G5\text{-}8}$) loops comprise the majority of the increased buried surface area and intermolecular contacts in the G5-8/SEB complex relative to the wild-type complex and form a contiguous interface with SEB centered around Asn60^{SEB} (Fig. 2c).

In protein–protein interactions, not all noncovalent contacts in the interface are energetically equivalent.[24,25] To determine which mutations in G5-8 resulted in significant energetic changes in complex formation with SEB, relative to the mVβ8.2/SEB complex, we assessed relative binding affinity changes for reversion mutations of each variant residue, as well as alanine and/or phenylalanine mutations of Tyr28$^{G5\text{-}8}$ and Arg53$^{G5\text{-}8}$ (see Supplementary Information, Materials and Methods). As others have combined phage display with alanine scanning mutagenesis to create "shotgun" alanine scanning mutagenesis,[26–28] we combined yeast display and reversion/replacement mutagenesis, as we had performed previously with another TCR/SAG interaction (hVβ2.1 in complex with toxic shock syndrome toxin-1[8]), for a facile and efficient method for the energetic evaluation of individual amino acid residues, or individual atoms thereof, in an evolved protein (Fig. 3a).

Using this approach, we found that several mutations in both the CDR1 loop and the CDR2 loop of G5-8 were energetically important for complex formation (Fig. 3b). Specifically, reversion mutations at CDR1 position 28 (Tyr28 → Asn; Fig. 3b, red) and CDR2 positions 52 through 54 (Ile52 → Ala, Arg53 → Gly, and Asn54 → Ser; Fig. 3b, blue) resulted in significant reductions in binding affinity when displayed on the yeast surface in the context of the G5-8 background.

To further dissect the molecular basis of affinity maturation in the CDR1 loop, we performed a similar mutagenesis analysis with Tyr28$^{G5\text{-}8}$ → Phe and Tyr28$^{G5\text{-}8}$ → Ala mutations. These two replacement mutations abrogate the hydrogen-bond and pi-stacking interactions, respectively, observed in the crystal structure (Fig. 2e). These assays indicated that the binding energy ascribed to Tyr28$^{G5\text{-}8}$ is derived primarily from the pi-stacking interaction between its phenyl ring and Arg110^{SEB}, and not from the hydrogen bond formed between its hydroxyl group and Asn60^{SEB} (Fig. 3b, red). Additionally, we observed no relative change in binding for the Ser27a$^{G5\text{-}8}$ → Ala mutation, confirming that this inserted residue does not itself make energetically significant interactions with SEB. Instead, the single-residue insertion at this position

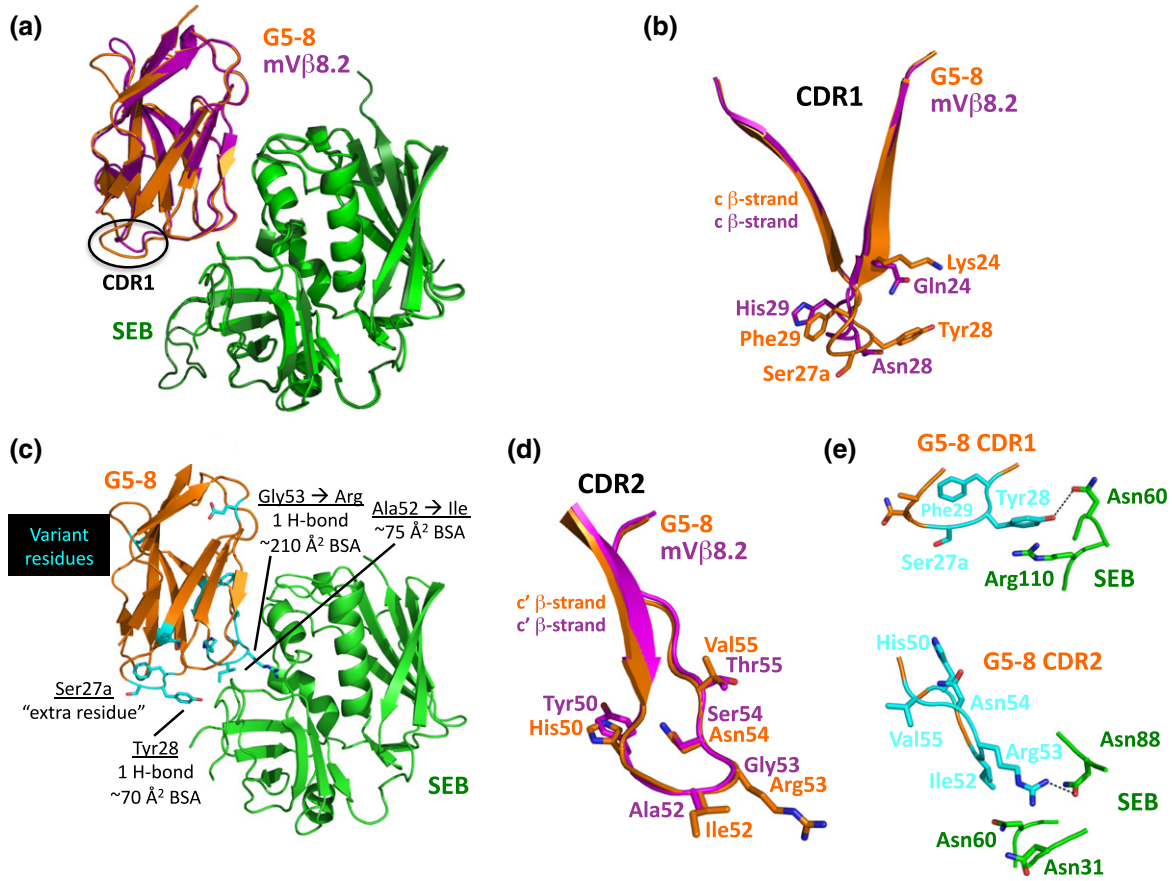

Fig. 2. Structural analysis of the affinity-matured complex. (a) Superposition of the wild-type mVβ8.2 (purple)/SEB (dark green) and G5-8 (orange)/SEB (light green) crystal structures. (b) The CDR1 loop structures of mVβ8.2 (purple) and G5-8 (orange), with side chains shown for variant residues. (c) Structure of G5-8 (orange; variant residues in cyan) in complex with SEB (green). (d) The CDR1 loop structures of mVβ8.2 (purple) and G5-8 (orange), with side chains shown for variant residues. (e) Intermolecular contacts between variant residues in G5-8 (cyan) and SEB (green) for both the CDR1 loop (top) and the CDR2 loop (bottom), with hydrogen bonds depicted.

probably acts as a spacer to lengthen the CDR1 loop such that $Tyr28^{G5\text{-}8}$ can form energetically productive contacts with SEB (see the text below).

The contiguous stretch of CDR2 loop residues 52 through 54 is critically important for affinity maturation (Fig. 3b, blue). The reversion mutation at position 53 contributes most significantly to the affinity maturation process, as might be expected from the ~ 210-Å increase in buried surface area that results from $Arg53^{G5\text{-}8}$ relative to that from $Gly53^{mV\beta8.2}$. Likewise, the ~75-Å increase in buried surface area that results from mutating $Ala52^{mV\beta8.2}$ to $Ile52^{G5\text{-}8}$ makes a significant contribution to binding in the G5-8/SEB complex. Although $Asn54^{G5\text{-}8}$ makes no intermolecular contacts with SEB, it may contribute to the affinity maturation process, perhaps through intramolecular interactions that act to stabilize the conformation of the G5-8 CDR2 loop. According to our mutational analysis, several other residues in both the CDR1 loop and the CDR2 loop (including $Lys24^{G5\text{-}8}$ and $Val55^{G5\text{-}8}$) may contribute to the affinity maturation process in a similar, although less significant, manner (Fig. 3b, gray). The molecular basis of affinity maturation by these residues is uncertain, but it may be due to effects on the conformational flexibility of the CDR loops, as suggested by an $Arg53^{G5\text{-}8}$-to-$Ala53^{G5\text{-}8}$ mutation that we observed to have an intermediate affinity between arginine and glycine residues at position 53. Based on our crystal structure, it is unlikely that the $Ala53^{G5\text{-}8}$ Cβ atom can contact SEB, indicating that CDR2 loop entropy and/or flexibility may contribute to G5-8/SEB binding.

In addition to the experimental mutational analysis described above, we performed a computational analysis of the same set of individual reversion and replacement mutations using the Rosetta program[29] (see Supplementary Information, Materials and Methods). The results of this computational analysis strongly corroborate the experimental results. A plot of Rosetta $\Delta\Delta G$ scores *versus* experimentally

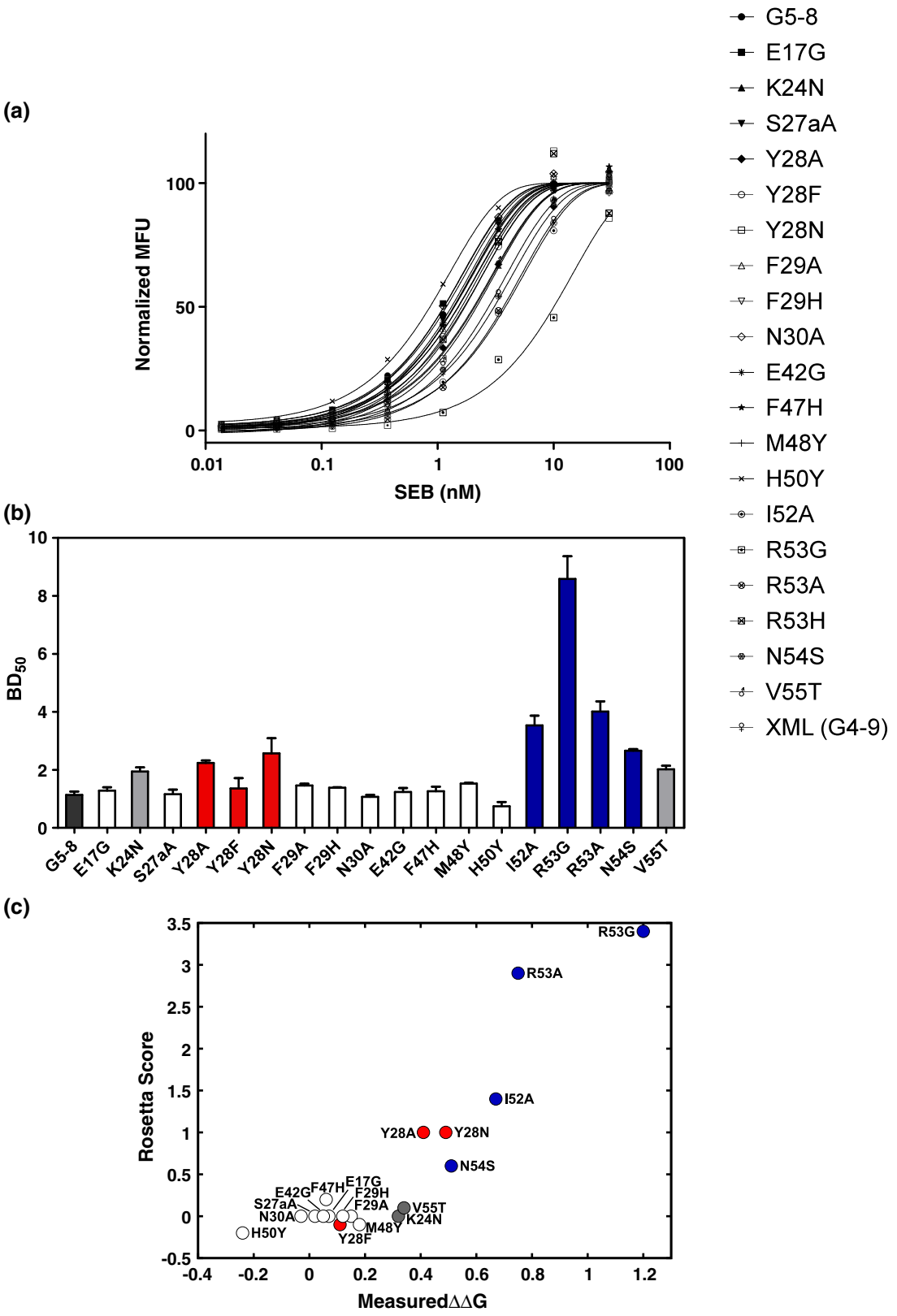

Fig. 3 (*legend on next page*)

measured binding free energies for all 18 CDR1 and CDR2 loop mutants (Fig. 3c) exhibits a correlation coefficient of 0.91. As with the experimental analysis, the computational analysis clearly distinguished those mutations that had profound *versus* insignificant binding effects and clearly implicated the pi-stacking interaction of Tyr28$^{G5\text{-}8}$ to be of greater energetic importance than the hydrogen bond formed between its hydroxyl group and Asn60^{SEB} (Supplementary Table 1). Only those residues for which we observed a small energetic effect experimentally, including Lys24$^{G5\text{-}8}$ and Val55$^{G5\text{-}8}$, were in poor agreement with the computational results. These residues do not make specific intermolecular contacts with SEB (Fig. 2e) and, thus, their energetic effects likely involve backbone conformational changes, as mentioned above, which are more difficult to model using computational algorithms.[30]

Computationally, we also assessed why the CDR1 residues in G5-8 may have given rise to a higher affinity and, therefore, selection in the final round of the directed evolution process. We found that, without the "spacer" residue Ser27a$^{G5\text{-}8}$, the tyrosine residue at position 28 makes very few, and no energetically favorable, contacts with SEB (Supplementary Table 2), supporting the need for CDR1 loop extension to achieve increased affinity. In addition, computational analysis revealed very few amino acids at position 28, other than tyrosine, to be energetically favorable in an extended CDR1 loop, with only tryptophan, phenylalanine (verified experimentally), and glutamic acid predicted to result in affinities commensurate to tyrosine at that position (Supplementary Table 2). The tryptophan is predicted to have favorable packing interactions in an orientation similar to that of Tyr28, while the modeled glutamic acid adopts a conformation for maximal electrostatic interactions with the positively charged side chain of Arg110 on SEB (Supplementary Fig. 4).

The structural and energetic changes that arise from our structure-based semirational directed evolution approach are entirely compatible with our original rationale for modifying the standard engineering strategy. Just as in the wild-type hVβ2.1/SpeC structure,[20] we find that lengthening the CDR1 loop of G5-8 by a single additional residue pushes a residue C-terminal to the insertion site closer towards SEB, with which it can form intermolecular contacts that significantly increase binding affinity. The evolution step of this approach is still required, however, as simply increasing the length of the wild-type CDR1 loop would not provide for these energetically productive interactions, since the wild-type residue Asn28$^{mV\beta8.2}$ would be unable to form similar pi-stacking or hydrogen-bond interactions with SEB. Thus, by rationalizing the directed evolution process in a structure-based manner to augment its evolutionary power, we have achieved an unprecedented level of affinity maturation in a protein–protein interaction that, in turn, resulted in a highly effective protein therapeutic.

Accession code

Coordinates and structure factors have been deposited in the Protein Data Bank under accession code 3R8B.

Acknowledgements

We thank Dr. Vivian Stojanoff for technical assistance at beamline X6A of the National Synchrotron Light Source. Use of the National Synchrotron Light Source, Brookhaven National Laboratory, was supported by the US Department of Energy, Office of Science, Office of Basic Energy Sciences, under contract no. DE-AC02-98CH10886. This work was supported, in part, by National Institutes of Health grants AI065690 (to E.J.S.), AI064611 (to D.M.K.), and GM084884 (to Z.W.).

Supplementary Data

Supplementary data to this article can be found online at doi:10.1016/j.jmb.2011.06.009

References

1. Holliger, P. & Hudson, P. J. (2005). Engineered antibody fragments and the rise of single domains. *Nat. Biotechnol.* **23**, 1126–1136.
2. Wittrup, K. D. (2001). Protein engineering by cell-surface display. *Curr. Opin. Biotechnol.* **12**, 395–399.

Fig. 3. Energetic dissection of the affinity-increasing mutations. (a) Titration binding curves for G5-8 and reversion/replacement mutants thereof, assayed by yeast display and normalized to G5-8 yeast surface expression. (b) Binding affinities of G5-8 and mutants thereof, as measured by yeast display flow titration. Energetically significant mutations are shown in red for CDR1 loop residues and in blue for CDR2 loop residues. Additional mutations that may potentially contribute to the affinity maturation process are shown in gray. (c) Computational analysis *versus* mutational analysis. Rosetta scores from computational analysis are plotted *versus* measured binding free energy changes ($\Delta\Delta G$), which were calculated as $RT*\ln(K_{mut}/K_{wt})$, with K_{wt} and K_{mut} from values in (b). The correlation coefficient (R) is 0.91. Color coding is the same as in (b).

3. Kolkman, J. A. & Stemmer, W. P. (2001). Directed evolution of proteins by exon shuffling. *Nat. Biotechnol.* **19**, 423–428.
4. Winter, G., Griffiths, A. D., Hawkins, R. E. & Hoogenboom, H. R. (1994). Making antibodies by phage display technology. *Annu. Rev. Immunol.* **12**, 433–455.
5. Eisen, H. N. (2001). Specificity and degeneracy in antigen recognition: yin and yang in the immune system. *Annu. Rev. Immunol.* **19**, 1–21.
6. Binz, H. K., Amstutz, P. & Pluckthun, A. (2005). Engineering novel binding proteins from nonimmunoglobulin domains. *Nat. Biotechnol.* **23**, 1257–1268.
7. Binz, H. K. & Pluckthun, A. (2005). Engineered proteins as specific binding reagents. *Curr. Opin. Biotechnol.* **16**, 459–469.
8. Buonpane, R. A., Moza, B., Sundberg, E. J. & Kranz, D. M. (2005). Characterization of T cell receptors engineered for high affinity against toxic shock syndrome toxin-1. *J. Mol. Biol.* **353**, 308–321.
9. Varela-Rohena, A., Molloy, P. E., Dunn, S. M., Li, Y., Suhoski, M. M., Carroll, R. G. *et al.* (2008). Control of HIV-1 immune escape by CD8 T cells expressing enhanced T-cell receptor. *Nat. Med.* **14**, 1390–1395.
10. Kieke, M. C., Sundberg, E., Shusta, E. V., Mariuzza, R. A., Wittrup, K. D. & Kranz, D. M. (2001). High affinity T cell receptors from yeast display libraries block T cell activation by superantigens. *J. Mol. Biol.* **307**, 1305–1315.
11. Koide, S. (2009). Generation of new protein functions by nonhomologous combinations and rearrangements of domains and modules. *Curr. Opin. Biotechnol.* **20**, 398–404.
12. Davis, M. M. & Bjorkman, P. J. (1988). T-cell antigen receptor genes and T-cell recognition. *Nature*, **334**, 395–402.
13. Lipovsek, D., Lippow, S. M., Hackel, B. J., Gregson, M. W., Cheng, P., Kapila, A. & Wittrup, K. D. (2007). Evolution of an interloop disulfide bond in high-affinity antibody mimics based on fibronectin type III domain and selected by yeast surface display: molecular convergence with single-domain camelid and shark antibodies. *J. Mol. Biol.* **368**, 1024–1041.
14. Hackel, B. J., Kapila, A. & Wittrup, K. D. (2008). Picomolar affinity fibronectin domains engineered utilizing loop length diversity, recursive mutagenesis, and loop shuffling. *J. Mol. Biol.* **381**, 1238–1252.
15. Koide, A., Gilbreth, R. N., Esaki, K., Tereshko, V. & Koide, S. (2007). High-affinity single-domain binding proteins with a binary-code interface. *Proc. Natl Acad. Sci. USA*, **104**, 6632–6637.
16. Xu, L., Aha, P., Gu, K., Kuimelis, R. G., Kurz, M., Lam, T. *et al.* (2002). Directed evolution of high-affinity antibody mimics using mRNA display. *Chem. Biol.* **9**, 933–942.
17. Buonpane, R. A., Churchill, H. R., Moza, B., Sundberg, E. J., Peterson, M. L., Schlievert, P. M. & Kranz, D. M. (2007). Neutralization of staphylococcal enterotoxin B by soluble, high-affinity receptor antagonists. *Nat. Med.* **13**, 725–729.
18. Malchiodi, E. L., Eisenstein, E., Fields, B. A., Ohlendorf, D. H., Schlievert, P. M., Karjalainen, K. & Mariuzza, R. A. (1995). Superantigen binding to a T cell receptor beta chain of known three-dimensional structure. *J. Exp. Med.* **182**, 1833–1845.
19. Leder, L., Llera, A., Lavoie, P. M., Lebedeva, M. I., Li, H., Sekaly, R. P. *et al.* (1998). A mutational analysis of the binding of staphylococcal enterotoxins B and C3 to the T cell receptor beta chain and major histocompatibility complex class II. *J. Exp. Med.* **187**, 823–833.
20. Sundberg, E. J., Li, H., Llera, A. S., McCormick, J. K., Tormo, J., Schlievert, P. M. *et al.* (2002). Structures of two streptococcal superantigens bound to TCR beta chains reveal diversity in the architecture of T cell signaling complexes. *Structure*, **10**, 687–699.
21. Li, H., Llera, A., Tsuchiya, D., Leder, L., Ysern, X., Schlievert, P. M. *et al.* (1998). Three-dimensional structure of the complex between a T cell receptor beta chain and the superantigen staphylococcal enterotoxin B. *Immunity*, **9**, 807–816.
22. Rahman, A. K., Herfst, C. A., Moza, B., Shames, S. R., Chau, L. A., Bueno, C. *et al.* (2006). Molecular basis of TCR selectivity, cross-reactivity, and allelic discrimination by a bacterial superantigen: integrative functional and energetic mapping of the SpeC–Vbeta2.1 molecular interface. *J. Immunol.* **177**, 8595–8603.
23. Churchill, H. R., Andersen, P. S., Parke, E. A., Mariuzza, R. A. & Kranz, D. M. (2000). Mapping the energy of superantigen *Staphylococcus* enterotoxin C3 recognition of an alpha/beta T cell receptor using alanine scanning mutagenesis. *J. Exp. Med.* **191**, 835–846.
24. Clackson, T. & Wells, J. A. (1995). A hot spot of binding energy in a hormone–receptor interface. *Science*, **267**, 383–386.
25. DeLano, W. L. (2002). Unraveling hot spots in binding interfaces: progress and challenges. *Curr. Opin. Struct. Biol.* **12**, 14–20.
26. Pal, G., Kossiakoff, A. A. & Sidhu, S. S. (2003). The functional binding epitope of a high affinity variant of human growth hormone mapped by shotgun alanine-scanning mutagenesis: insights into the mechanisms responsible for improved affinity. *J. Mol. Biol.* **332**, 195–204.
27. Vajdos, F. F., Adams, C. W., Breece, T. N., Presta, L. G., de Vos, A. M. & Sidhu, S. S. (2002). Comprehensive functional maps of the antigen-binding site of an anti-ErbB2 antibody obtained with shotgun scanning mutagenesis. *J. Mol. Biol.* **320**, 415–428.
28. Weiss, G. A., Watanabe, C. K., Zhong, A., Goddard, A. & Sidhu, S. S. (2000). Rapid mapping of protein functional epitopes by combinatorial alanine scanning. *Proc. Natl Acad. Sci. USA*, **97**, 8950–8954.
29. Kortemme, T. & Baker, D. (2002). A simple physical model for binding energy hot spots in protein–protein complexes. *Proc. Natl Acad. Sci. USA*, **99**, 14116–14121.
30. Mandell, D. J. & Kortemme, T. (2009). Computer-aided design of functional protein interactions. *Nat. Chem. Biol.* **5**, 797–807.